Upper limits on a stochastic gravitational-wave background using LIGO and Virgo interferometers at 600–1000 Hz

J. Abadie,[1,a] B. P. Abbott,[1,a] R. Abbott,[1,a] T. D. Abbott,[2,a] M. Abernathy,[3,a] T. Accadia,[4,b] F. Acernese,[5a,5c,b] C. Adams,[6,a] R. Adhikari,[1,a] C. Affeldt,[7,8,a] M. Agathos,[9a,b] K. Agatsuma,[10,a] P. Ajith,[1,a] B. Allen,[7,11,8,a] E. Amador Ceron,[11,a] D. Amariutei,[12,a] S. B. Anderson,[1,a] W. G. Anderson,[11,a] K. Arai,[1,a] M. A. Arain,[12,a] M. C. Araya,[1,a] S. M. Aston,[13,a] P. Astone,[14a,b] D. Atkinson,[15,a] P. Aufmuth,[8,7,a] C. Aulbert,[7,8,a] B. E. Aylott,[13,a] S. Babak,[16,a] P. Baker,[17,a] G. Ballardin,[18,b] S. Ballmer,[19,a] J. C. B. Barayoga,[1,a] D. Barker,[15,a] F. Barone,[5a,5c,b] B. Barr,[3,a] L. Barsotti,[20,a] M. Barsuglia,[21,b] M. A. Barton,[15,a] I. Bartos,[22,a] R. Bassiri,[3,a] M. Bastarrika,[3,a] A. Basti,[23a,23b,b] J. Batch,[15,a] J. Bauchrowitz,[7,8,a] Th. S. Bauer,[9a,b] M. Bebronne,[4,b] D. Beck,[24,a] B. Behnke,[16,a] M. Bejger,[25c,b] M. G. Beker,[9a,b] A. S. Bell,[3,a] A. Belletoile,[4,b] I. Belopolski,[22,a] M. Benacquista,[26,a] J. M. Berliner,[15,a] A. Bertolini,[7,8,a] J. Betzwieser,[1,a] N. Beveridge,[3,a] P. T. Beyersdorf,[27,a] I. A. Bilenko,[28,a] G. Billingsley,[1,a] J. Birch,[6,a] R. Biswas,[26,a] M. Bitossi,[23a,b] M. A. Bizouard,[29a,b] E. Black,[1,a] J. K. Blackburn,[1,a] L. Blackburn,[30,a] D. Blair,[31,a] B. Bland,[15,a] M. Blom,[9a,b] O. Bock,[7,8,a] T. P. Bodiya,[20,a] C. Bogan,[7,8,a] R. Bondarescu,[32,a] F. Bondu,[33b,b] L. Bonelli,[23a,23b,b] R. Bonnand,[34,b] R. Bork,[1,a] M. Born,[7,8,a] V. Boschi,[23a,b] S. Bose,[35,a] L. Bosi,[36a,b] B. Bouhou,[21,b] S. Braccini,[23a,b] C. Bradaschia,[23a,b] P. R. Brady,[11,a] V. B. Braginsky,[28,a] M. Branchesi,[37a,37b,b] J. E. Brau,[38,a] J. Breyer,[7,8,a] T. Briant,[39,b] D. O. Bridges,[6,a] A. Brillet,[33a,b] M. Brinkmann,[7,8,a] V. Brisson,[29a,b] M. Britzger,[7,8,a] A. F. Brooks,[1,a] D. A. Brown,[19,a] T. Bulik,[25b,b] H. J. Bulten,[9a,9b,b] A. Buonanno,[40,a] J. Burguet–Castell,[41,a] D. Buskulic,[4,b] C. Buy,[21,b] R. L. Byer,[24,a] L. Cadonati,[42,a] G. Cagnoli,[37a,b] E. Calloni,[5a,5b,b] J. B. Camp,[30,a] P. Campsie,[3,a] J. Cannizzo,[30,a] K. Cannon,[43,a] B. Canuel,[18,b] J. Cao,[44,a] C. D. Capano,[19,a] F. Carbognani,[18,b] L. Carbone,[13,a] S. Caride,[45,a] S. Caudill,[46,a] M. Cavaglià,[47,a] F. Cavalier,[29a,b] R. Cavalieri,[18,b] G. Cella,[23a,b] C. Cepeda,[1,a] E. Cesarini,[37b,b] O. Chaibi,[33a,b] T. Chalermsongsak,[1,a] P. Charlton,[48,a] E. Chassande-Mottin,[21,b] S. Chelkowski,[13,a] W. Chen,[44,a] X. Chen,[31,a] Y. Chen,[49,a] A. Chincarini,[50,b] A. Chiummo,[18,b] H. S. Cho,[51,a] J. Chow,[52,a] N. Christensen,[53,a] S. S. Y. Chua,[52,a] C. T. Y. Chung,[54,a] S. Chung,[31,a] G. Ciani,[12,a] F. Clara,[15,a] D. E. Clark,[24,a] J. Clark,[55,a] J. H. Clayton,[11,a] F. Cleva,[33a,b] E. Coccia,[56a,56b,b] P.-F. Cohadon,[39,b] C. N. Colacino,[23a,23b,b] J. Colas,[18,b] A. Colla,[14a,14b,b] M. Colombini,[14b,b] A. Conte,[14a,14b,b] R. Conte,[57,a] D. Cook,[15,a] T. R. Corbitt,[20,a] M. Cordier,[27,a] N. Cornish,[17,a] A. Corsi,[1,a] C. A. Costa,[46,a] M. Coughlin,[53,a] J.-P. Coulon,[33a,b] P. Couvares,[19,a] D. M. Coward,[31,a] M. Cowart,[6,a] D. C. Coyne,[1,a] J. D. E. Creighton,[11,a] T. D. Creighton,[26,a] A. M. Cruise,[13,a] A. Cumming,[3,a] L. Cunningham,[3,a] E. Cuoco,[18,b] R. M. Cutler,[13,a] K. Dahl,[7,8,a] S. L. Danilishin,[28,a] R. Dannenberg,[1,a] S. D'Antonio,[56a,b] K. Danzmann,[7,8,a] V. Dattilo,[18,b] B. Daudert,[1,a] H. Daveloza,[26,a] M. Davier,[29a,b] E. J. Daw,[58,a] R. Day,[18,b] T. Dayanga,[35,a] R. De Rosa,[5a,5b,b] D. DeBra,[24,a] G. Debreczeni,[59,b] W. Del Pozzo,[9a,b] M. del Prete,[60b,b] T. Dent,[55,a] V. Dergachev,[1,a] R. DeRosa,[46,a] R. DeSalvo,[1,a] S. Dhurandhar,[61,a] L. Di Fiore,[5a,b] A. Di Lieto,[23a,23b,b] I. Di Palma,[7,8,a] M. Di Paolo Emilio,[56a,56c,b] A. Di Virgilio,[23a,b] M. Díaz,[26,a] A. Dietz,[4,b] F. Donovan,[20,a] K. L. Dooley,[12,a] M. Drago,[60a,60b,b] R. W. P. Drever,[62,a] J. C. Driggers,[1,a] Z. Du,[44,a] J.-C. Dumas,[31,a] S. Dwyer,[20,a] T. Eberle,[7,8,a] M. Edgar,[3,a] M. Edwards,[55,a] A. Effler,[46,a] P. Ehrens,[1,a] G. Endrőczi,[59,b] R. Engel,[1,a] T. Etzel,[1,a] K. Evans,[3,a] M. Evans,[20,a] T. Evans,[6,a] M. Factourovich,[22,a] V. Fafone,[56a,56b,b] S. Fairhurst,[55,a] Y. Fan,[31,a] B. F. Farr,[63,a] D. Fazi,[63,a] H. Fehrmann,[7,8,a] D. Feldbaum,[12,a] F. Feroz,[64,a] I. Ferrante,[23a,23b,b] F. Fidecaro,[23a,23b,b] L. S. Finn,[32,a] I. Fiori,[18,b] R. P. Fisher,[32,a] R. Flaminio,[34,b] M. Flanigan,[15,a] S. Foley,[20,a] E. Forsi,[6,a] L. A. Forte,[5a,b] N. Fotopoulos,[1,a] J.-D. Fournier,[33a,b] J. Franc,[34,b] S. Frasca,[14a,14b,b] F. Frasconi,[23a,b] M. Frede,[7,8,a] M. Frei,[65,66,a] Z. Frei,[67,a] A. Freise,[13,a] R. Frey,[38,a] T. T. Fricke,[46,a] D. Friedrich,[7,8,a] P. Fritschel,[20,a] V. V. Frolov,[6,a] M.-K. Fujimoto,[10,a] P. J. Fulda,[13,a] M. Fyffe,[6,a] J. Gair,[64,a] M. Galimberti,[34,b] L. Gammaitoni,[36a,36b,b] J. Garcia,[15,a] F. Garufi,[5a,5b,b] M. E. Gáspár,[59,b] G. Gemme,[50,b] R. Geng,[44,a] E. Genin,[18,b] A. Gennai,[23a,b] L. Á. Gergely,[68,a] S. Ghosh,[35,a] J. A. Giaime,[46,6,a] S. Giampanis,[11,a] K. D. Giardina,[6,a] A. Giazotto,[23a,b] S. Gil-Casanova,[41,a] C. Gill,[3,a] J. Gleason,[12,a] E. Goetz,[7,8,a] L. M. Goggin,[11,a] G. González,[46,a] M. L. Gorodetsky,[28,a] S. Goßler,[7,8,a] R. Gouaty,[4,b] C. Graef,[7,8,a] P. B. Graff,[64,a] M. Granata,[21,b] A. Grant,[3,a] S. Gras,[31,a] C. Gray,[15,a] N. Gray,[3,a] R. J. S. Greenhalgh,[69,a] A. M. Gretarsson,[70,a] C. Greverie,[33a,b] R. Grosso,[26,a] H. Grote,[7,8,a] S. Grunewald,[16,a] G. M. Guidi,[37a,37b,b] C.. Guido,[6,a] R. Gupta,[61,a] E. K. Gustafson,[1,a] R. Gustafson,[45,a] T. Ha,[71,a] J. M. Hallam,[13,a] D. Hammer,[11,a] G. Hammond,[3,a] J. Hanks,[15,a] C. Hanna,[1,72,a] J. Hanson,[6,a] J. Harms,[62,a] G. M. Harry,[20,a] I. W. Harry,[55,a] E. D. Harstad,[38,a] M. T. Hartman,[12,a] K. Haughian,[3,a] K. Hayama,[10,a] J.-F. Hayau,[33b,b] J. Heefner,[1,a] A. Heidmann,[39,b] M. C. Heintze,[12,a] H. Heitmann,[33a,b] P. Hello,[29a,b] M. A. Hendry,[3,a] I. S. Heng,[3,a] A. W. Heptonstall,[1,a] V. Herrera,[24,a] M. Hewitson,[7,8,a] S. Hild,[3,a] D. Hoak,[42,a] K. A. Hodge,[1,a] K. Holt,[6,a] M. Holtrop,[73,a] T. Hong,[49,a] S. Hooper,[31,a] D. J. Hosken,[74,a] J. Hough,[3,a] E. J. Howell,[31,a] B. Hughey,[11,a] S. Husa,[41,a] S. H. Huttner,[3,a] T. Huynh-Dinh,[6,a] D. R. Ingram,[15,a] R. Inta,[52,a] T. Isogai,[53,a] A. Ivanov,[1,a] K. Izumi,[10,a] M. Jacobson,[1,a] E. James,[1,a] Y. J. Jang,[44,a] P. Jaranowski,[25d,b] E. Jesse,[70,a] W. W. Johnson,[46,a] D. I. Jones,[75,a] G. Jones,[55,a] R. Jones,[3,a] L. Ju,[31,a]

P. Kalmus,[1,a] V. Kalogera,[63,a] S. Kandhasamy,[76,a] G. Kang,[77,a] J. B. Kanner,[40,a] R. Kasturi,[78,a] E. Katsavounidis,[20,a] W. Katzman,[6,a] H. Kaufer,[7,8,a] K. Kawabe,[15,a] S. Kawamura,[10,a] F. Kawazoe,[7,8,a] D. Kelley,[19,a] W. Kells,[1,a] D. G. Keppel,[1,a] Z. Keresztes,[68,a] A. Khalaidovski,[7,8,a] F. Y. Khalili,[28,a] E. A. Khazanov,[79,a] B. K. Kim,[77,a] C. Kim,[80,a] H. Kim,[7,8,a] K. Kim,[81,a] N. Kim,[24,a] Y. M. Kim,[51,a] P. J. King,[1,a] D. L. Kinzel,[6,a] J. S. Kissel,[20,a] S. Klimenko,[12,a] K. Kokeyama,[13,a] V. Kondrashov,[1,a] S. Koranda,[11,a] W. Z. Korth,[1,a] I. Kowalska,[25b,b] D. Kozak,[1,a] O. Kranz,[7,8,a] V. Kringel,[7,8,a] S. Krishnamurthy,[63,a] B. Krishnan,[16,a] A. Królak,[25a,25e,b] G. Kuehn,[7,8,a] R. Kumar,[3,a] P. Kwee,[8,7,a] P. K. Lam,[52,a] M. Landry,[15,a] B. Lantz,[24,a] N. Lastzka,[7,8,a] C. Lawrie,[3,a] A. Lazzarini,[1,a] P. Leaci,[16,a] C. H. Lee,[51,a] H. K. Lee,[81,a] H. M. Lee,[82,a] J. R. Leong,[7,8,a] I. Leonor,[38,a] N. Leroy,[29a,b] N. Letendre,[4,b] J. Li,[44,a] T. G. F. Li,[9a,b] N. Liguori,[60a,60b,b] P. E. Lindquist,[1,a] Y. Liu,[44,a] Z. Liu,[12,a] N. A. Lockerbie,[83,a] D. Lodhia,[13,a] M. Lorenzini,[37a,b] V. Loriette,[29b,b] M. Lormand,[6,a] G. Losurdo,[37a,b] J. Lough,[19,a] J. Luan,[49,a] M. Lubinski,[15,a] H. Lück,[7,8,a] A. P. Lundgren,[32,a] E. Macdonald,[3,a] B. Machenschalk,[7,8,a] M. MacInnis,[20,a] D. M. Macleod,[55,a] M. Mageswaran,[1,a] K. Mailand,[1,a] E. Majorana,[14a,b] I. Maksimovic,[29b,b] N. Man,[33a,b] I. Mandel,[20,a] V. Mandic,[76,a] M. Mantovani,[23a,23c,b] A. Marandi,[24,a] F. Marchesoni,[36a,b] F. Marion,[4,b] S. Márka,[22,a] Z. Márka,[22,a] A. Markosyan,[24,a] E. Maros,[1,a] J. Marque,[18,b] F. Martelli,[37a,37b,b] I. W. Martin,[3,a] R. M. Martin,[12,a] J. N. Marx,[1,a] K. Mason,[20,a] A. Masserot,[4,b] F. Matichard,[20,a] L. Matone,[22,a] R. A. Matzner,[65,a] N. Mavalvala,[20,a] G. Mazzolo,[7,8,a] R. McCarthy,[15,a] D. E. McClelland,[52,a] S. C. McGuire,[84,a] G. McIntyre,[1,a] J. McIver,[42,a] D. J. A. McKechan,[55,a] S. McWilliams,[22,a] G. D. Meadors,[45,a] M. Mehmet,[7,8,a] T. Meier,[8,7,a] A. Melatos,[54,a] A. C. Melissinos,[85,a] G. Mendell,[15,a] R. A. Mercer,[11,a] S. Meshkov,[1,a] C. Messenger,[55,a] M. S. Meyer,[6,a] H. Miao,[49,a] C. Michel,[34,b] L. Milano,[5a,5b,b] J. Miller,[52,a] Y. Minenkov,[56a,b] V. P. Mitrofanov,[28,a] G. Mitselmakher,[12,a] R. Mittleman,[20,a] O. Miyakawa,[10,a] B. Moe,[11,a] M. Mohan,[18,b] S. D. Mohanty,[26,a] S. R. P. Mohapatra,[42,a] D. Moraru,[15,a] G. Moreno,[15,a] N. Morgado,[34,b] A. Morgia,[56a,56b,b] T. Mori,[10,a] S. R. Morriss,[26,a] S. Mosca,[5a,5b,b] K. Mossavi,[7,8,a] B. Mours,[4,b] C. M. Mow–Lowry,[52,a] C. L. Mueller,[12,a] G. Mueller,[12,a] S. Mukherjee,[26,a] A. Mullavey,[52,a] H. Müller-Ebhardt,[7,8,a] J. Munch,[74,a] D. Murphy,[22,a] P. G. Murray,[3,a] A. Mytidis,[12,a] T. Nash,[1,a] L. Naticchioni,[14a,14b,b] V. Necula,[12,a] J. Nelson,[3,a] I. Neri,[3,b] G. Newton,[3,a] T. Nguyen,[52,a] A. Nishizawa,[10,a] A. Nitz,[19,a] F. Nocera,[18,b] D. Nolting,[6,a] M. E. Normandin,[26,a] L. Nuttall,[55,a] E. Ochsner,[40,a] J. O'Dell,[69,a] E. Oelker,[20,a] G. H. Ogin,[1,a] J. J. Oh,[71,a] S. H. Oh,[71,a] B. O'Reilly,[6,a] R. O'Shaughnessy,[11,a] C. Osthelder,[1,a] C. D. Ott,[49,a] D. J. Ottaway,[74,a] R. S. Ottens,[12,a] H. Overmier,[6,a] B. J. Owen,[32,a] A. Page,[13,a] G. Pagliaroli,[56a,56c,b] L. Palladino,[56a,56c,b] C. Palomba,[14a,b] Y. Pan,[40,a] C. Pankow,[12,a] F. Paoletti,[23a,18,b] M. A. Papa,[16,11,a] M. Parisi,[5a,5b,b] A. Pasqualetti,[18,b] R. Passaquieti,[23a,23b,b] D. Passuello,[23a,b] P. Patel,[1,a] M. Pedraza,[1,a] P. Peiris,[66,a] L. Pekowsky,[19,a] S. Penn,[78,a] A. Perreca,[19,a] G. Persichetti,[5a,5b,b] M. Phelps,[1,a] M. Pichot,[1,b] M. Pickenpack,[7,8,a] F. Piergiovanni,[37a,37b,b] M. Pietka,[25d,b] L. Pinard,[34,b] I. M. Pinto,[86,a] M. Pitkin,[3,a] H. J. Pletsch,[7,8,a] M. V. Plissi,[3,a] R. Poggiani,[23a,23b,b] J. Pöld,[7,8,a] F. Postiglione,[57,a] M. Prato,[50,b] V. Predoi,[55,a] T. Prestegard,[76,a] L. R. Price,[1,a] M. Prijatelj,[7,8,a] M. Principe,[86,a] S. Privitera,[1,a] R. Prix,[7,8,a] G. A. Prodi,[60a,60b,b] L. G. Prokhorov,[28,a] O. Puncken,[7,8,a] M. Punturo,[36a,b] P. Puppo,[14a,b] V. Quetschke,[26,a] R. Quitzow-James,[38,a] F. J. Raab,[15,a] D. S. Rabeling,[9a,9b,b] I. Rácz,[59,b] H. Radkins,[15,a] P. Raffai,[67,a] M. Rakhmanov,[26,a] B. Rankins,[47,a] P. Rapagnani,[14a,14b,b] V. Raymond,[63,a] V. Re,[56a,56b,b] K. Redwine,[22,a] C. M. Reed,[15,a] T. Reed,[87,a] T. Regimbau,[33a,b] S. Reid,[3,a] D. H. Reitze,[12,a] F. Ricci,[14a,14b,b] R. Riesen,[6,a] K. Riles,[45,a] N. A. Robertson,[1,3,a] F. Robinet,[29a,b] C. Robinson,[55,a] E. L. Robinson,[16,a] A. Rocchi,[56a,b] S. Roddy,[6,a] C. Rodriguez,[63,a] M. Rodruck,[15,a] L. Rolland,[4,b] J. G. Rollins,[1,a] J. D. Romano,[26,a] R. Romano,[5a,5c,b] J. H. Romie,[6,a] D. Rosińska,[25c,25f,b] C. Röver,[7,8,a] S. Rowan,[3,a] A. Rüdiger,[7,8,a] P. Ruggi,[18,b] K. Ryan,[15,a] P. Sainathan,[12,a] F. Salemi,[7,8,a] L. Sammut,[54,a] V. Sandberg,[15,a] V. Sannibale,[1,a] L. Santamaría,[1,a] I. Santiago-Prieto,[3,a] G. Santostasi,[88,a] B. Sassolas,[34,b] B. S. Sathyaprakash,[55,a] S. Sato,[10,a] P. R. Saulson,[19,a] R. L. Savage,[15,a] R. Schilling,[7,8,a] R. Schnabel,[7,8,a] R. M. S. Schofield,[38,a] E. Schreiber,[7,8,a] B. Schulz,[7,8,a] B. F. Schutz,[16,55,a] P. Schwinberg,[15,a] J. Scott,[3,a] S. M. Scott,[52,a] F. Seifert,[1,a] D. Sellers,[6,a] D. Sentenac,[18,b] A. Sergeev,[79,a] D. A. Shaddock,[52,a] M. Shaltev,[7,8,a] B. Shapiro,[20,a] P. Shawhan,[40,a] D. H. Shoemaker,[20,a] A. Sibley,[6,a] X. Siemens,[11,a] D. Sigg,[15,a] A. Singer,[1,a] L. Singer,[1,a] A. M. Sintes,[41,a] G. R. Skelton,[11,a] B. J. J. Slagmolen,[52,a] J. Slutsky,[46,a] J. R. Smith,[2,a] M. R. Smith,[1,a] R. J. E. Smith,[13,a] N. D. Smith-Lefebvre,[15,a] K. Somiya,[49,a] B. Sorazu,[3,a] J. Soto,[20,a] F. C. Speirits,[3,a] L. Sperandio,[56a,56b,b] M. Stefszky,[52,a] A. J. Stein,[20,a] L. C. Stein,[20,a] E. Steinert,[15,a] J. Steinlechner,[7,8,a] S. Steinlechner,[7,8,a] S. Steplewski,[35,a] A. Stochino,[1,a] R. Stone,[26,a] K. A. Strain,[3,a] S. E. Strigin,[28,a] A. S. Stroeer,[26,a] R. Sturani,[37a,37b,b] A. L. Stuver,[6,a] T. Z. Summerscales,[89,a] M. Sung,[46,a] S. Susmithan,[31,a] P. J. Sutton,[55,a] B. Swinkels,[18,b] M. Tacca,[18,b] L. Taffarello,[60c,b] D. Talukder,[35,a] D. B. Tanner,[12,a] S. P. Tarabrin,[7,8,a] J. R. Taylor,[7,8,a] R. Taylor,[1,a] P. Thomas,[15,a] K. A. Thorne,[6,a] K. S. Thorne,[49,a] E. Thrane,[76,a] A. Thüring,[8,7,a] K. V. Tokmakov,[83,a] C. Tomlinson,[58,a] A. Toncelli,[23a,23b,b] M. Tonelli,[23a,23b,b] O. Torre,[23a,23c,b] C. Torres,[6,a] C. I. Torrie,[1,3,a] E. Tournefier,[4,b] F. Travasso,[36a,36b,b] G. Traylor,[6,a] K. Tseng,[24,a] D. Ugolini,[90,a] H. Vahlbruch,[8,7,a] G. Vajente,[23a,23b,b] J. F. J. van den Brand,[9a,9b,b] C. Van Den Broeck,[9a,b]

S. van der Putten,[9a,b] A. A. van Veggel,[3,a] S. Vass,[1,a] M. Vasuth,[59,b] R. Vaulin,[20,a] M. Vavoulidis,[29a,b] A. Vecchio,[13,a] G. Vedovato,[60c,b] J. Veitch,[55,a] P. J. Veitch,[74,a] C. Veltkamp,[7,8,a] D. Verkindt,[4,b] F. Vetrano,[37a,37b,b] A. Viceré,[37a,37b,b] A. E. Villar,[1,a] J.-Y. Vinet,[33a,b] S. Vitale,[9a,b] H. Vocca,[36a,b] C. Vorvick,[15,a] S. P. Vyatchanin,[28,a] A. Wade,[52,a] L. Wade,[11,a] M. Wade,[11,a] S. J. Waldman,[20,a] L. Wallace,[1,a] Y. Wan,[44,a] M. Wang,[13,a] X. Wang,[44,a] Z. Wang,[44,a] A. Wanner,[7,8,a] R. L. Ward,[21,b] M. Was,[29a,b] M. Weinert,[7,8,a] A. J. Weinstein,[1,a] R. Weiss,[20,a] L. Wen,[49,31,a] P. Wessels,[7,8,a] M. West,[19,a] T. Westphal,[7,8,a] K. Wette,[7,8,a] J. T. Whelan,[66,a] S. E. Whitcomb,[1,31,a] D. J. White,[58,a] B. F. Whiting,[12,a] C. Wilkinson,[15,a] P. A. Willems,[1,a] L. Williams,[12,a] R. Williams,[1,a] B. Willke,[7,8,a] L. Winkelmann,[7,8,a] W. Winkler,[7,8,a] C. C. Wipf,[20,a] A. G. Wiseman,[11,a] H. Wittel,[7,8,a] G. Woan,[3,a] R. Wooley,[6,a] J. Worden,[15,a] I. Yakushin,[6,a] H. Yamamoto,[1,a] K. Yamamoto,[7,8,60b,60d,a,b] C. C. Yancey,[40,a] H. Yang,[49,a] D. Yeaton-Massey,[1,a] S. Yoshida,[91,a] P. Yu,[11,a] M. Yvert,[4,b] A. Zadrożny,[25e,b] M. Zanolin,[70,a] J.-P. Zendri,[60c,b] F. Zhang,[44,a] L. Zhang,[1,a] W. Zhang,[44,a] C. Zhao,[31,a] N. Zotov,[87,a] M. E. Zucker,[20,a] and J. Zweizig[1,a]

([a]LIGO Scientific Collaboration)
([b]Virgo Collaboration)

[1]*LIGO-California Institute of Technology, Pasadena, California 91125, USA*
[2]*California State University Fullerton, Fullerton California 92831 USA*
[3]*SUPA, University of Glasgow, Glasgow, G12 8QQ, United Kingdom*
[4]*Laboratoire d'Annecy-le-Vieux de Physique des Particules (LAPP), Université de Savoie, CNRS/IN2P3, F-74941 Annecy-Le-Vieux, France*
[5a]*INFN, Sezione di Napoli, Italy*
[5b]*Università di Napoli 'Federico II', Italy*
[5c]*Complesso Universitario di Monte S. Angelo, I-80126 Napoli and Università di Salerno, Fisciano, I-84084 Salerno, Italy*
[6]*LIGO-Livingston Observatory, Livingston, Louisiana 70754, USA*
[7]*Albert-Einstein-Institut, Max-Planck-Institut für Gravitationsphysik, D-30167 Hannover, Germany*
[8]*Leibniz Universität Hannover, D-30167 Hannover, Germany*
[9a]*Nikhef, Science Park, Amsterdam, the Netherlands*
[9b]*VU University Amsterdam, De Boelelaan 1081, 1081 HV Amsterdam, the Netherlands*
[10]*National Astronomical Observatory of Japan, Tokyo 181-8588, Japan*
[11]*University of Wisconsin-Milwaukee, Milwaukee, Wisconsin 53201, USA*
[12]*University of Florida, Gainesville, Florida 32611, USA*
[13]*University of Birmingham, Birmingham, B15 2TT, United Kingdom*
[14a]*INFN, Sezione di Roma, I-00185 Roma, Italy*
[14b]*Università 'La Sapienza', I-00185 Roma, Italy*
[15]*LIGO-Hanford Observatory, Richland, Washington 99352, USA*
[16]*Albert-Einstein-Institut, Max-Planck-Institut für Gravitationsphysik, D-14476 Golm, Germany*
[17]*Montana State University, Bozeman, Montana 59717, USA*
[18]*European Gravitational Observatory (EGO), I-56021 Cascina (PI), Italy*
[19]*Syracuse University, Syracuse, New York 13244, USA*
[20]*LIGO-Massachusetts Institute of Technology, Cambridge, Massachusetts 02139, USA*
[21]*Laboratoire AstroParticule et Cosmologie (APC) Université Paris Diderot, CNRS: IN2P3, CEA: DSM/IRFU, Observatoire de Paris, 10 rue A. Domon et L. Duquet, 75013 Paris-France*
[22]*Columbia University, New York, New York 10027, USA*
[23a]*INFN, Sezione di Pisa, I-56127 Pisa, Italy*
[23b]*Università di Pisa, I-56127 Pisa, Italy*
[23c]*Università di Siena, I-53100 Siena, Italy*
[24]*Stanford University, Stanford, California 94305, USA*
[25a]*IM-PAN, 00-956 Warsaw, Poland*
[25b]*Astronomical Observatory Warsaw University, 00-478 Warsaw, Poland*
[25c]*CAMK-PAN, 00-716 Warsaw, Poland*
[25d]*Białystok University, 15-424 Białystok, Poland*
[25e]*IPJ, 05-400 Świerk-Otwock, Poland*
[25f]*Institute of Astronomy, 65-265 Zielona Góra, Poland*
[26]*The University of Texas at Brownsville and Texas Southmost College, Brownsville, Texas 78520, USA*
[27]*San Jose State University, San Jose, California 95192, USA*
[28]*Moscow State University, Moscow, 119992, Russia*
[29a]*LAL, Université Paris-Sud, IN2P3/CNRS, F-91898 Orsay, France*
[29b]*ESPCI, CNRS, F-75005 Paris, France*

[30]*NASA/Goddard Space Flight Center, Greenbelt, Maryland 20771, USA*
[31]*University of Western Australia, Crawley, WA 6009, Australia*
[32]*The Pennsylvania State University, University Park, Pennsylvania 16802, USA*
[33a]*Université Nice-Sophia-Antipolis, CNRS, Observatoire de la Côte d'Azur, F-06304 Nice, France*
[33b]*Institut de Physique de Rennes, CNRS, Université de Rennes 1, 35042 Rennes, France*
[34]*Laboratoire des Matériaux Avancés (LMA), IN2P3/CNRS, F-69622 Villeurbanne, Lyon, France*
[35]*Washington State University, Pullman, Washington 99164, USA*
[36a]*INFN, Sezione di Perugia, I-06123 Perugia, Italy*
[36b]*Università di Perugia, I-06123 Perugia, Italy*
[37a]*INFN, Sezione di Firenze, I-50019 Sesto Fiorentino, Italy*
[37b]*Università degli Studi di Urbino 'Carlo Bo', I-61029 Urbino, Italy*
[38]*University of Oregon, Eugene, Oregon 97403, USA*
[39]*Laboratoire Kastler Brossel, ENS, CNRS, UPMC, Université Pierre et Marie Curie, 4 Place Jussieu, F-75005 Paris, France*
[40]*University of Maryland, College Park, Maryland 20742 USA*
[41]*Universitat de les Illes Balears, E-07122 Palma de Mallorca, Spain*
[42]*University of Massachusetts-Amherst, Amherst, Massachusetts 01003, USA*
[43]*Canadian Institute for Theoretical Astrophysics, University of Toronto, Toronto, Ontario, M5S 3H8, Canada*
[44]*Tsinghua University, Beijing 100084 China*
[45]*University of Michigan, Ann Arbor, Michigan 48109, USA*
[46]*Louisiana State University, Baton Rouge, Louisiana 70803, USA*
[47]*The University of Mississippi, University, Mississippi 38677, USA*
[48]*Charles Sturt University, Wagga Wagga, NSW 2678, Australia*
[49]*Caltech-CaRT, Pasadena, California 91125, USA*
[50]*INFN, Sezione di Genova, I-16146 Genova, Italy*
[51]*Pusan National University, Busan 609-735, Korea*
[52]*Australian National University, Canberra, ACT 0200, Australia*
[53]*Carleton College, Northfield, Minnesota 55057, USA*
[54]*The University of Melbourne, Parkville, VIC 3010, Australia*
[55]*Cardiff University, Cardiff, CF24 3AA, United Kingdom*
[56a]*INFN, Sezione di Roma Tor Vergata, Italy*
[56b]*Università di Roma Tor Vergata, I-00133 Roma, Italy*
[56c]*Università dell'Aquila, I-67100 L'Aquila, Italy*
[57]*University of Salerno, I-84084 Fisciano (Salerno), Italy and INFN (Sezione di Napoli), Italy*
[58]*The University of Sheffield, Sheffield S10 2TN, United Kingdom*
[59]*RMKI, H-1121 Budapest, Konkoly Thege Miklós út 29-33, Hungary*
[60a]*INFN, Gruppo Collegato di Trento, I-38050 Povo, Trento, Italy*
[60b]*Università di Trento, I-38050 Povo, Trento, Italy*
[60c]*INFN, Sezione di Padova, I-35131 Padova, Italy*
[60d]*Università di Padova, I-35131 Padova, Italy*
[61]*Inter-University Centre for Astronomy and Astrophysics, Pune-411007, India*
[62]*California Institute of Technology, Pasadena, California 91125, USA*
[63]*Northwestern University, Evanston, Illinois 60208, USA*
[64]*University of Cambridge, Cambridge, CB2 1TN, United Kingdom*
[65]*The University of Texas at Austin, Austin, Texas 78712, USA*
[66]*Rochester Institute of Technology, Rochester, New York 14623, USA*
[67]*Eötvös Loránd University, Budapest, 1117 Hungary*
[68]*University of Szeged, 6720 Szeged, Dóm tér 9, Hungary*
[69]*Rutherford Appleton Laboratory, HSIC, Chilton, Didcot, Oxon OX11 0QX United Kingdom*
[70]*Embry-Riddle Aeronautical University, Prescott, Arizona 86301 USA*
[71]*National Institute for Mathematical Sciences, Daejeon 305-390, Korea*
[72]*Perimeter Institute for Theoretical Physics, Ontario, N2L 2Y5, Canada*
[73]*University of New Hampshire, Durham, New Hampshire 03824, USA*
[74]*University of Adelaide, Adelaide, SA 5005, Australia*
[75]*University of Southampton, Southampton, SO17 1BJ, United Kingdom*
[76]*University of Minnesota, Minneapolis, Minnesota 55455, USA*
[77]*Korea Institute of Science and Technology Information, Daejeon 305-806, Korea*
[78]*Hobart and William Smith Colleges, Geneva, New York 14456, USA*
[79]*Institute of Applied Physics, Nizhny Novgorod, 603950, Russia*
[80]*Lund Observatory, Box 43, SE-221 00, Lund, Sweden*
[81]*Hanyang University, Seoul 133-791, Korea*
[82]*Seoul National University, Seoul 151-742, Korea*

[83]University of Strathclyde, Glasgow, G1 1XQ, United Kingdom
[84]Southern University and A&M College, Baton Rouge, Louisiana 70813, USA
[85]University of Rochester, Rochester, New York 14627, USA
[86]University of Sannio at Benevento, I-82100 Benevento, Italy and INFN (Sezione di Napoli), Italy
[87]Louisiana Tech University, Ruston, Louisiana 71272, USA
[88]McNeese State University, Lake Charles, Louisiana 70609 USA
[89]Andrews University, Berrien Springs, Michigan 49104 USA
[90]Trinity University, San Antonio, Texas 78212, USA
[91]Southeastern Louisiana University, Hammond, Louisiana 70402, USA
(Received 29 January 2012; published 4 June 2012)

A stochastic background of gravitational waves is expected to arise from a superposition of many incoherent sources of gravitational waves, of either cosmological or astrophysical origin. This background is a target for the current generation of ground-based detectors. In this article we present the first joint search for a stochastic background using data from the LIGO and Virgo interferometers. In a frequency band of 600–1000 Hz, we obtained a 95% upper limit on the amplitude of $\Omega_{\mathrm{GW}}(f) = \Omega_3(f/900\ \mathrm{Hz})^3$, of $\Omega_3 < 0.32$, assuming a value of the Hubble parameter of $h_{100} = 0.71$. These new limits are a factor of seven better than the previous best in this frequency band.

DOI: 10.1103/PhysRevD.85.122001 PACS numbers: 95.85.Sz, 04.30.Db, 04.80.Nn, 07.05.Kf

I. INTRODUCTION

A major science goal of current and future generations of gravitational-wave detectors is the detection of a stochastic gravitational-wave background (SGWB)—a superposition of unresolvable gravitational-wave signals of astrophysical and/or cosmological origin. An astrophysical background is expected to be comprised of signals originating from astrophysical objects, for example, binary neutron stars [1], spinning neutron stars [2], magnetars [3], or core-collapse supernovae [4]. A cosmological background is expected to be generated by various physical processes in the early universe [5] and, as gravitational waves are so weakly interacting, to be essentially unattenuated since then. We expect that gravitational waves would decouple much earlier than other radiation, so a cosmological background would carry the earliest information accessible about the very early universe [6]. There are various production mechanisms from which we might expect cosmological gravitational waves including cosmic strings [7], amplification of vacuum fluctuations following inflation [8,9], pre-Big-Bang models [10,11], or the electroweak phase transition [12].

Whatever the production mechanism of a SGWB, the signal is usually described in terms of the dimensionless quantity,

$$\Omega_{\mathrm{GW}}(f) = \frac{f}{\rho_c}\frac{d\rho_{\mathrm{GW}}}{df}, \tag{1}$$

where $d\rho_{\mathrm{GW}}$ is the energy density of gravitational radiation contained in the frequency range f to $f + df$ and ρ_c is the critical energy density of the universe [13]. As a SGWB signal is expected to be much smaller than current detector noise, and because we assume both the detector noise and the signal to be Gaussian random variables, it is not feasible to distinguish the two in a single interferometer. We must therefore search for the SGWB using two or more interferometers. The optimal method is to cross-correlate the strain data from a pair, or several pairs of detectors [13]. In recent years, several interferometric gravitational-wave detectors have been in operation in the USA and Europe. At the time that the data analyzed in this paper were taken, five interferometers were in operation. Two LIGO interferometers were located at the same site in Hanford, WA, one with 4 km arms and one with 2 km arms (referred to as H1 and H2, respectively). In addition, one LIGO 4 km interferometer, L1, was located in Livingston, LA [14]. The Virgo interferometer, V1, with 3 km arms was located near Pisa, Italy [15] and GEO600, with 600 m arms, was located near Hannover, Germany [16]. LIGO carried out its fifth science run, along with GEO600, between 5th November 2005 and 30th September 2007. They were joined from 18th May 2007 by Virgo, carrying out its first science run. In this paper we present a joint analysis of the data taken by the LIGO and Virgo detectors during these periods, in the frequency range 600–1000 Hz. This is the first search for a SGWB using data from both LIGO and Virgo interferometers, and the first using multiple baselines. Previous searches using the LIGO interferometers used just one baseline. The most sensitive direct limit obtained so far used the three LIGO interferometers, but as the two Hanford interferometers were collocated this involved just one baseline [17]. The most recent upper limit in frequency band studied in this paper was obtained using data from the LIGO-Livingston interferometer and the ALLEGRO bar detector, which were collocated for the duration of the analysis [18]. The addition of Virgo to the LIGO interferometers adds two further baselines, for which the frequency dependence of the sensitivity varies differently. The frequency range used in this paper was chosen because the addition of Virgo data was expected to most improve the sensitivity at these high frequencies. This is due in part to the relative orientation and separation of

the LIGO and Virgo interferometers, and in part to the fact that the Virgo sensitivity is closest to the LIGO sensitivity at these frequencies. The GEO600 interferometer was not included in this analysis as the strain sensitivity at these frequencies was insufficient to significantly improve the sensitivity of the search.

The structure of this paper is as follows. In Sec. II we describe the method used to analyze the data. In Sec. III we present the results of the analysis of data from the LIGO and Virgo interferometers. We describe validation of the results using software injections in Sec. IV. In Sec. V we compare our results to those of previous experiments and in Sec. VI we summarize our conclusions.

II. ANALYSIS METHOD

The output of an interferometer is assumed to be the sum of instrumental noise and a stochastic background signal,

$$s(t) = n(t) + h(t). \tag{2}$$

The gravitational-wave signal has a power spectrum, $S_{\mathrm{GW}}(f)$, which is related to $\Omega_{\mathrm{GW}}(f)$ by [19]

$$S_{\mathrm{GW}}(f) = \frac{3H_0^2}{10\pi^2}\frac{\Omega_{\mathrm{GW}}(f)}{f^3}. \tag{3}$$

Our signal model is a power law spectrum,

$$\Omega_{\mathrm{GW}}(f) = \Omega_\alpha\left(\frac{f}{f_R}\right)^\alpha, \tag{4}$$

where α is the spectral index, and f_R a reference frequency, such that $\Omega_\alpha = \Omega_{\mathrm{GW}}(f_R)$. For this analysis we create a filter using a model which corresponds to a white strain amplitude spectrum and choose a reference frequency of 900 Hz, such that

$$\Omega_{\mathrm{GW}}(f) = \Omega_3\left(\frac{f}{900\ \mathrm{Hz}}\right)^3. \tag{5}$$

We choose this spectrum as it is expected that some astrophysical backgrounds will have a rising $\Omega_{\mathrm{GW}}(f)$ spectrum in the frequency band we are investigating [2–4]. In fact, different models predict different values of the spectral index α in our frequency band, so we quote upper limits for several values.

For a pair of detectors, with interferometers labeled by i and j, we calculate the cross-correlation statistic in the frequency domain

$$\begin{aligned}\hat{Y} &= \int_{-\infty}^{+\infty} df Y(f) \\ &= \int_{-\infty}^{+\infty} df \int_{-\infty}^{+\infty} df' \delta_T(f-f')\tilde{s}_i^\star(f)\tilde{s}_j(f')\tilde{Q}_{ij}(f'),\end{aligned} \tag{6}$$

where $\tilde{s}_i(f)$ and $\tilde{s}_j(f)$ are the Fourier transforms of the strain time-series of two interferometers, $\tilde{Q}_{ij}(f)$ is a filter function, and δ_T is a finite-time approximation to the Dirac delta function, [13]

$$\delta_T(f) := \int_{-T/2}^{T/2} dt e^{-i2\pi ft} = \frac{\sin(\pi fT)}{\pi f}. \tag{7}$$

We assume the detector noise is Gaussian, stationary, uncorrelated between the two interferometers and much larger than the signal. Under these assumptions, the variance of the estimator $\hat{Y}$ is

$$\sigma_{\hat{Y}}^2 = \int_0^{+\infty} df \sigma_{\hat{Y}}^2(f) \approx \frac{T}{2}\int_0^{+\infty} df P_i(f)P_j(f) \mid \tilde{Q}_{ij}(f)|^2, \tag{8}$$

where $P_i(f)$ is the one-sided power spectral density of interferometer i and T is the integration time. By maximizing the expected signal-to-noise ratio (SNR) for a chosen model of $\Omega_{\mathrm{GW}}(f)$, we find the optimal filter function,

$$\tilde{Q}_{ij}(f) = \mathcal{N}\frac{\gamma_{ij}(f)f^{\alpha-3}}{f_R^\alpha P_i(f)P_j(f)}, \tag{9}$$

where $\gamma_{ij}(f)$ is the overlap reduction function (ORF) of the two interferometers and $\mathcal{N}$ is a normalization factor. We choose the normalization such that the cross-correlation statistic is an estimator of Ω_α, with expectation value $\langle\hat{Y}\rangle = \Omega_\alpha$. It follows that the normalization is

$$\mathcal{N} = \frac{f_R^{2\alpha}}{T}\left(\frac{10\pi^2}{3H_0^2}\right)\left[\int_0^\infty df \frac{f^{2\alpha-6}\gamma_{ij}^2(f)}{P_i(f)P_j(f)}\right]^{-1}. \tag{10}$$

Using this filter function and normalization gives an optimal SNR of [13]

$$\mathrm{SNR} \approx \frac{3H_0^2}{10\pi^2}\sqrt{2T}\left[\int_0^\infty df \frac{\gamma_{ij}^2(f)\Omega_{GW}^2(f)}{f^6 P_i(f)P_j(f)}\right]^{1/2}. \tag{11}$$

The ORF encodes the separation and orientations of the detectors and is defined as [13,20]

$$\gamma_{ij}(f) := \frac{5}{8\pi}\sum_A \int_{S^2} d\hat{\Omega} e^{i2\pi f\hat{\Omega}\cdot\Delta\vec{x}/c} F_i^A(\hat{\Omega})F_j^A(\hat{\Omega}), \tag{12}$$

where $\hat{\Omega}$ is a unit vector specifying a direction on the two-sphere, $\Delta\vec{x} = \vec{x}_i - \vec{x}_j$ is the separation of the two interferometers and

$$F_i^A(\hat{\Omega}) = e_{ab}^A(\hat{\Omega})d_i^{ab} \tag{13}$$

is the response of the ith detector to the $A = +,\times$ polarization, where e_{ab}^A are the transverse traceless polarization tensors. The geometry of each interferometer is described by a response tensor,

$$d^{ab} = \frac{1}{2}(\hat{x}^a\hat{x}^b - \hat{y}^a\hat{y}^b), \tag{14}$$

which is constructed from the two unit vectors that point along the arms of the interferometer, $\hat{x}$ and $\hat{y}$ [20,21]. At zero frequency, the ORF is determined solely by the relative orientations of the two interferometers. The LIGO

interferometers are oriented in such a way as to maximize the amplitude of the ORF at low frequency, while the relative orientations of the LIGO-Virgo pairs are poor. Thus at low frequency the amplitude of the ORF between the Hanford and Livingston interferometers, $\gamma_{\mathrm{HL}}(f)$, is larger than that of the overlap between Virgo and any of the LIGO interferometers, $\gamma_{\mathrm{HV}}(f)$ or $\gamma_{\mathrm{LV}}(f)$ (note that the ''HL'' and ''HV'' overlap reduction functions hold for both H1 and H2 as they are collocated). However, at high frequency the ORF behaves as a sinc function of the frequency multiplied by the light-travel time between the interferometers. As the LIGO interferometers are closer to each other than to Virgo, their ORF $\gamma_{\mathrm{HL}}(f)$ oscillates less, but decays more rapidly with frequency than the the ORFs of the LIGO-Virgo pairs. Figure 1 shows the ORFs between the LIGO-Hanford, LIGO-Livingston, and Virgo sites.

We define the ''sensitivity integrand'', $\mathcal{I}(f)$, by inserting Eqs. (9) and (10) into Eq. (8), giving

$$\sigma_Y^2 = \left(\int_0^\infty \mathcal{I}(f)df\right)^{-1} = \frac{f_R^{2\alpha}}{8T}\left(\frac{10\pi^2}{3H_0^2}\right)^2\left(\int_0^\infty df\,\frac{\gamma_{ij}^2(f)f^{2\alpha-6}}{P_i(f)P_j(f)}\right)^{-1}. \quad (15)$$

This demonstrates the contribution to the inverse of the variance at each frequency. The sensitivity of each pair is dependent on the noise power spectra of the two interferometers, as well as the observing geometry, described by $\gamma_{ij}(f)$. For interferometers operating at design sensitivity, this means that for frequencies above ~200 Hz the LIGO-Virgo pairs make the dominant contribution to the sensitivity [22]. During its first science run Virgo was closest to design sensitivity at frequencies above several hundred Hz, which informed our decision to use the 600–1000 Hz band.

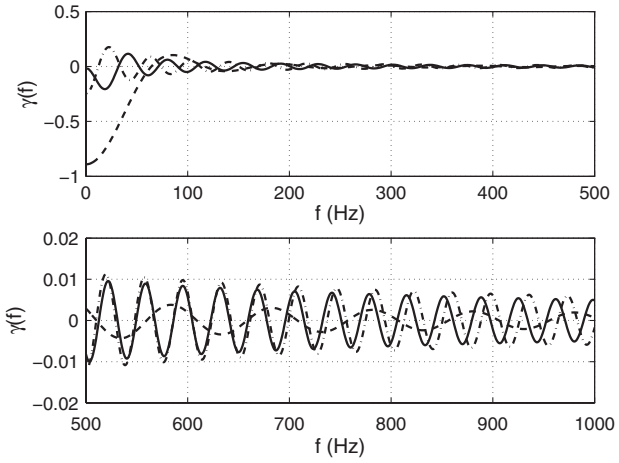

FIG. 1. Plot of the overlap reduction function (ORF) for the pairs of sites used in this analysis. The dashed curve is the ORF for the two LIGO sites (HL), the solid curve is for the Hanford-Virgo sites (HV), and the dashed-dotted curve is for Livingston-Virgo (LV). We see that the LIGO orientations have been optimized for low-frequency searches, around 10–100 Hz. However, this ORF falls off rapidly with frequency, such that at frequencies over ~500 Hz, the amplitude of the ORF of the HL pair is smaller than that of the Virgo pairs. The LV and HV overlap reduction functions oscillate more with frequency, but fall off more slowly, due to the larger light-travel time between the USA and Europe.

The procedure by which we analyzed the data is as follows. For each pair of interferometers, labeled by I, the coincident data were divided into segments, labeled by J, of length $T = 60$ s. The data from each segment are Hann windowed in order to minimize spectral leakage. In order not to reduce the effective observation time, the segments are therefore overlapped by 50%. For each segment, the data from both interferometers were Fourier transformed then coarse-grained to a resolution of 0.25 Hz. The data from the adjacent segments were then used to calculate power spectral densities (PSDs) with Welch's method. The Fourier transformed data and the PSDs were used to calculate the estimator on Ω_3, $\hat{Y}_{IJ}$, and its standard deviation, σ_{IJ}. For each pair, the results from all segments were optimally combined by performing a weighted average (with weights $1/\sigma_{IJ}^2$), taking into account the correlations that were introduced by the overlapping segments [23]. The weighted average for each pair, $\hat{Y}_I$, has an associated standard deviation σ_I, also calculated by combining the standard deviations from each segment (note that σ_I is the equivalent of σ_Y [from Eq. (8)] for each pair, I, but we have dropped the Y subscript to simplify the notation).

A. Data quality

Data quality cuts were made to eliminate data that was too noisy or nonstationary, or that had correlated noise between detectors. Time segments that were known to contain large noise transients in one interferometer were removed from the analysis. We also excluded times when the digitizers were saturated, times with particularly high noise, and times when the calibration was unreliable. This also involved excluding the last thirty seconds before the loss of lock in the interferometers, as they are known to have an increase in noise in this period. Additionally, we ensured that the data were approximately stationary over a period of three minutes, as the PSD estimates, $P_i(f)$, used in calculating the optimal filter and standard deviation in each segment are obtained from data in the immediately adjacent segments. This was achieved by calculating a measure of stationarity,

$$\Delta\sigma_{IJ} = \frac{|\sigma_{IJ} - \sigma'_{IJ}|}{\sigma_{IJ}}, \quad (16)$$

for each segment, where σ_{IJ} was calculated [following Eq. (8)] using the PSDs estimated from the adjacent segments, and σ'_{IJ} was calculated using the PSDs estimated using data from the segment itself. To ensure stationarity,

we set a threshold value, ζ, and all segments with values of $\Delta\sigma_{IJ} > \zeta$ are discarded. The threshold was tuned by analyzing the data with unphysical time offsets between the interferometers; a value of $\zeta = 0.1$ as this ensures that the remaining data are Gaussian.

In order to exclude correlations between the instruments caused by environmental factors we excluded certain frequencies from our analysis. The frequency bins to be removed were identified in two ways. Some correlations between the interferometers were known to exist *a priori*, e.g. there are correlations at multiples of 60 Hz between the interferometers located in the USA due to the frequency of the power supply [19]. These were removed from the analysis, but in order to ensure that all coherent bins were identified, we also calculated the coherence,

$$\Gamma(f) = \frac{|\tilde{s}_1^\star(f)\tilde{s}_2(f)|^2}{P_1(f)P_2(f)}, \tag{17}$$

which is the ratio of the cross-spectrum to the product of the two power spectral densities, averaged over the whole run. This value was calculated first at a resolution of 0.1 Hz, then at 1 mHz to investigate in more detail the frequency distribution of the coherence. Several frequencies showed excess coherence; some had been identified *a priori* but two had not, so these were also removed from the analysis. The calculations of the power spectra and the cross correlation were carried out at a resolution of 0.25 Hz, so we removed the corresponding 0.25 Hz bin from our analysis. Excess coherence was defined as coherence exceeding a threshold of $\Gamma(f) = 5 \times 10^{-3}$. This threshold was also chosen after analyzing the data with unphysical time offsets. The excluded bins for each interferometer can be seen in Table I.

TABLE I. Table of the frequency bins excluded from the analysis for each interferometer. The bins at 640 Hz and 961 Hz were identified using coherence tests, while the others were excluded *a priori*. Also excluded were harmonics of the power line frequency at multiples of 60 Hz for the LIGO detectors and multiples of 50 Hz for Virgo. Each excluded bin is centered at the frequency listed above and has a width of 0.25 Hz.

IFO	Notched frequencies (Hz)	
H1	786.25	Harmonic of calibration line
	961	Timing diagnostic line
H2	640	Excess noise
	814.5	Harmonic of calibration line
	961	Timing diagnostic line
L1	793.5	Harmonic of calibration line
	961	Timing diagnostic line
V1	706	
	710	Harmonics of
	714	calibration lines
	718	

B. Timing accuracy

In order to be sure that the cross correlation is a measure of the gravitational-wave signal present in both detectors in a pair, we must be sure that the data collected in both detectors are truly coincident. Calibration studies were carried out to determine the timing offset, if any, between the detectors and to estimate the error on this offset. These studies are described in more detail in Ref. [24], but we summarize them here.

The output of each interferometer is recorded at a rate of 16 384 Hz. Each data point has an associated time-stamp and we need to ensure that data taken with identical time-stamps are indeed coincident measurements of the strain, to within the calibration errors of the instruments. No offset between the instruments was identified, but several possible sources of timing error were investigated. First, approximations in our models of the interferometers can introduce phase errors. For the measurement of strain, we model the interferometers using the long-wavelength approximation (i.e. we assume that the wavelengths of the gravitational waves that we measure are much longer than the arm-lengths of the interferometers). We also make an approximation in the transfer function of the Fabry-Perot cavity; the exact function has several poles or singularities, but we use an approximation which includes only the lowest frequency pole [25]. The errors that these two approximations introduce largely cancel, with a residual error of ~ 2 μs or $\sim 1°$ at 1 kHz [24].

Second, there is some propagation time between strain manifesting in the detectors and the detector output being recorded in a frame file. This is well understood for all detectors and is accounted for (to within calibration errors) when the detector outputs are converted to strain. The time-stamp associated with each data point is therefore taken to be the GPS time at which the differential arm length occurs, to within calibration errors [24].

Third, the GPS time recorded at each site has some uncertainty. The timing precision of the GPS system is $\sim$30 ns, which corresponds with the stated location accuracy of $\sim$10 m. Each site necessarily uses its own GPS receiver, so the relative accuracy of these receivers has been checked, by taking a Virgo GPS receiver to a LIGO site and comparing the outputs. The relative accuracy was found to be better than 1 μs. The receivers have also been checked against Network Time Protocol (NTP) and were found to have no offset [24]. The total error in GPS timing is far smaller than the instrumental phase calibration errors in the 600–1000 Hz frequency band (see Table II).

These investigations concluded that the timing offset between the instruments is zero for all pairs, with errors on these values that are smaller than the error in the phase calibration of each instrument. The phase calibration errors of the instruments are negligible in this analysis as their inclusion would produce a smaller than 1% change in the

TABLE II. Table of values of the errors in the calibration of amplitude and phase for each of the LIGO [26] and Virgo [27] instruments used in this analysis. The errors are valid over the whole 600–1000 Hz band.

Instrument	Amplitude error (%)	Phase error (degrees)
H1	10.2	4.3
H2	10.3	3.4
L1	13.4	2.3
V1	6.0	4.0

results at this sensitivity, and therefore the relative timing error is negligible.

C. Combination of multiple pairs

We performed an analysis of all of the available data from LIGO's fifth science run and Virgo's first science run. However, we excluded the H1–H2 pair as the two instruments were built inside the same vacuum system, and so may have significant amounts of correlated noise. There is an ongoing investigation into identifying and removing these correlations [28], and for the present analysis, we consider only the five remaining pairs. As described above, the output of each pair yields an estimator, $\hat{Y}_I$, with a standard deviation, σ_I, where $I = 1 \ldots 5$ labels the detector pair.

Using the estimators $\hat{Y}_I$ and their associated error bars, σ_I, we construct a Bayesian posterior probability density function (PDF) on Ω_3. Bayes theorem says that the posterior PDF of a set of unknown parameters, $\vec{\theta}$, given a set of data, $\mathcal{D}$, is given by

$$p(\vec{\theta}|\mathcal{D}) = \frac{p(\vec{\theta})p(\mathcal{D}|\vec{\theta})}{p(\mathcal{D})}, \tag{18}$$

where $p(\vec{\theta})$ is the prior PDF on the unknown parameters—representing the state of knowledge before the experiment-$p(\mathcal{D}|\vec{\theta})$ is the likelihood function and $p(\mathcal{D})$ is a normalization factor. In this case, the unknown parameters, $\vec{\theta}$, are the value of Ω_3 and the amplitude calibration factors of the instruments, which will be discussed below. The data set, $\mathcal{D}$, is the set of five estimators, $\{\hat{Y}_I\}$, we obtain from the five pairs of instruments.

In forming this posterior, we must consider the errors in the calibration of the strain data obtained by the interferometers. In the data from one interferometer, labeled by i, there may be an error on the calibration of both the amplitude and the phase, such that the value we measure is

$$\tilde{s}_i(f) = e^{\Lambda_i + i\phi_i}\tilde{s}_i^t(f), \tag{19}$$

where $\tilde{s}_i^t(f)$ is the "true" value that would be measured if the interferometer were perfectly calibrated. The phase calibration errors given in Table II are negligible, and the studies described in Sec. II B have shown that there is no significant relative timing error between the interferometers, so we can simply assume that $\phi_i = 0$. However, the amplitude calibration errors are not negligible, and the calibration factors take the values $\Lambda_i = 0 \pm \epsilon_{\Lambda,i}$, where $\epsilon_{\Lambda,i}$ are the fractional amplitude calibration errors of the instruments, which are quoted in Table II.

The calibration factors combine such that the estimator for a pair I is

$$\hat{Y}_I = e^{\Lambda_{I,1}+\Lambda_{I,2}}\hat{Y}_I^t, \tag{20}$$

where $\hat{Y}_I^t$ is the true value that would be measured with perfectly calibrated instruments and $\Lambda_{I,1}$ and $\Lambda_{I,2}$ are the calibration factors of the two instruments in pair I. The likelihood function for a single estimator is given by

$$p(\hat{Y}_I|\Omega_3, \sigma_I, \Lambda_I) = \frac{1}{\sigma_I\sqrt{2\pi}}\exp\left(-\frac{(\hat{Y}_I - e^{\Lambda_I}\Omega_3)^2}{2\sigma_I^2}\right), \tag{21}$$

where we have used $\Lambda_I = \Lambda_{I,1} + \Lambda_{I,2}$. The joint likelihood function on all the data is the product over all pairs of Eq. (21)

$$p(\{\hat{Y}_I\}|\Omega_3, \{\sigma_I\}, \{\Lambda_I\}) = \prod_{I=1}^{n_{\text{pairs}}} p(\hat{Y}_I|\Omega_3, \sigma_I, \Lambda_I). \tag{22}$$

In order to form a posterior PDF, we define priors on the calibration factors of the individual interferometers, $\{\Lambda_i\}$. The calibration factors are assumed to be Gaussian distributed, with variance given by the square of the calibration errors quoted in Table II, such that

$$p(\{\Lambda_i\}|\{\epsilon_{\Lambda,i}\}) = \prod_{i=1}^{n_{\text{IFO}}}\frac{1}{\epsilon_{\Lambda,i}\sqrt{2\pi}}\exp\left(-\frac{\Lambda_i^2}{2\epsilon_{\Lambda,i}^2}\right), \tag{23}$$

where n_{IFO} is the number of interferometers we are using, in this case four. The prior on Ω_3 is a top hat function

$$p(\Omega_3) = \begin{cases} \frac{1}{\Omega_{\max}} & \text{for } 0 \le \Omega < \Omega_{\max} \\ 0 & \text{otherwise} \end{cases}. \tag{24}$$

We choose a flat prior on Ω_3 because, although there has been an analysis in this band previously, it did not include data from the whole of the frequency band and an uninformative flat prior is conservative. We chose $\Omega_{\max} = 10$, which is two orders of magnitude greater than the estimators and their standard deviations, such that the prior is essentially unconstrained.

We combine the prior and likelihood functions to give a posterior PDF

$$p(\Omega_3, \{\Lambda_i\}|\{\hat{Y}_I\}, \{\sigma_I\}, \{\epsilon_{\Lambda,i}\}) = p(\Omega_3)p(\{\Lambda_i\}|\{\epsilon_{\Lambda,i}\})p(\{\hat{Y}_I\}|\Omega_3, \{\sigma_I\}, \{\Lambda_I\}). \tag{25}$$

We marginalize this posterior analytically over all Λ_i [36] to give us a posterior on Ω_3 alone,

$$p(\Omega_3|\{\hat{Y}_I\},\{\sigma_I\},\{\epsilon_{\Lambda,i}\}) = \int_{-\infty}^{\infty} d\Lambda_1 \int_{-\infty}^{\infty} d\Lambda_2 \ldots \times \int_{-\infty}^{\infty} d\Lambda_{n_{\rm IFO}} p(\Omega_3,\{\Lambda_i\}|\{\hat{Y}_I\},\times\{\sigma_I\},\{\epsilon_{\Lambda,i}\}). \quad (26)$$

Using this posterior PDF we calculate a 95% probability interval, $(\Omega_{\rm lower}, \Omega_{\rm upper})$ on Ω_3. We calculate the values of $\Omega_{\rm lower}$ and $\Omega_{\rm upper}$ by finding the minimum-width interval that satisfies

$$\int_{\Omega_{\rm lower}}^{\Omega_{\rm upper}} p(\Omega_3|\{\hat{Y}_I\},\{\sigma_I\},\{\epsilon_{\Lambda,i}\}) d\Omega_3 = 0.95. \quad (27)$$

If we find that $\Omega_{\rm lower}$ is equal to zero, then we have a null result, and we can simply quote the upper limit, $\Omega_{\rm upper}$.

The optimal estimator, $\hat{Y}$, is given by the combination of Y_I, σ_I and Λ_I that maximizses the likelihood, such that

$$\hat{Y} = \frac{\sum_I e^{\Lambda_I} \hat{Y}_I \sigma_I^{-2}}{\sum_I e^{2\Lambda_I} \sigma_I^{-2}}. \quad (28)$$

It has a variance, σ, given by

$$\sigma^{-2} = \sum_I e^{2\Lambda_I} \sigma_I^{-2}. \quad (29)$$

Under the assumption that the calibration factors Λ_i are all equal to zero, then the optimal way to combine the results from each pair is to perform a weighted average with weights $1/\sigma_I^2$ (equivalently to combining results from multiple, uncorrelated, time segments) [22]

$$\hat{Y} = \frac{\sum_I \hat{Y}_I \sigma_I^{-2}}{\sum_I \sigma_I^{-2}} \quad (30)$$

$$\sigma^{-2} = \sum_I \sigma_I^{-2}. \quad (31)$$

A combined sensitivity integrand can also be found by summing the integrands from each pair: [22]

$$\mathcal{I}(f) = \sum_I \mathcal{I}_I(f) \quad (32)$$

III. RESULTS

We applied the analysis described in Sec. II to all of the available data from the LIGO and Virgo interferometers between November 2005 and September 2007[1] and obtained estimators of Ω_3 from each of five pairs, which are listed in Table III along with their standard deviations. We also create the combined estimators and their standard deviations, using Eqs. (30) and (31), for the full network, and for the network including only the LIGO interferometers. We see that the addition of Virgo to the network reduces the size of the standard deviation by 23%.

TABLE III. Table of values of $\hat{Y}_I$, the estimator of Ω_3, obtained by analyzing the data taken during LIGO's fifth science run and Virgo's first science run, over a frequency band of 600–1000 Hz, along with the standard deviation, σ_I, of each result.

Network	Estimator $\hat{Y}_I$
H1L1	0.11 ± 0.15
H1V1	0.55 ± 0.21
H2L1	-0.14 ± 0.25
H2V1	-0.51 ± 0.40
L1V1	0.18 ± 0.19
LIGO	0.05 ± 0.13
all	0.15 ± 0.10

Using the posterior PDF defined in Eq. (26) and the calibration errors in Table II we found a 95% upper limit of $\Omega_3 < 0.32$, assuming the Hubble constant to be $h_{100} = 0.71$ [29] (see also [30]). while using only the LIGO instruments obtained an upper limit of $\Omega_3 < 0.30$. Both of the lower limits were zero. The posterior PDFs obtained by the search are shown in Fig. 2, while the sensitivity integrands, which show the contribution to the sensitivity of the search from each frequency bin, are shown in Fig. 3. The upper limit corresponds to a strain sensitivity of 8.5×10^{-24} Hz$^{-1/2}$ using just the LIGO interferometers, or 8.7×10^{-24} Hz$^{-1/2}$ using both LIGO and Virgo. The LIGO-only upper limit is, in fact, lower than the upper

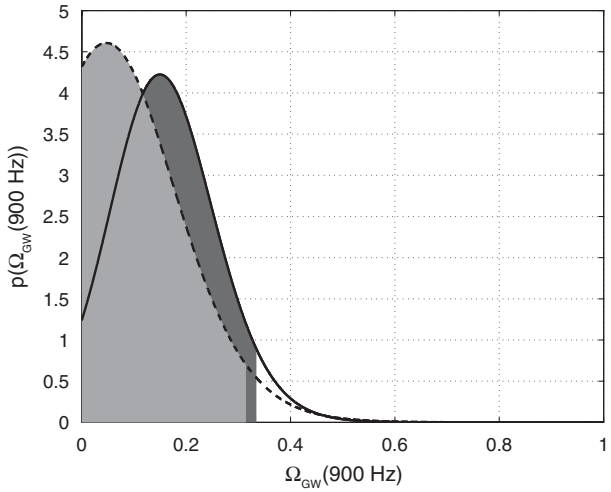

FIG. 2. Posterior PDFs on Ω_3. The dashed line shows the posterior PDF obtained using just the LIGO detectors, the solid line shows the PDF obtained using LIGO and Virgo detectors. The filled areas show the 95% probability intervals.

[1]We initially analyzed only data from times after Virgo had begun taking data (May–September 2007). This preliminary analysis resulted in a marginal signal with a false-alarm probability of $p = 2\%$. To follow up, we extended the analysis to include all available LIGO data, yielding the results shown here, which are consistent with the null hypothesis.

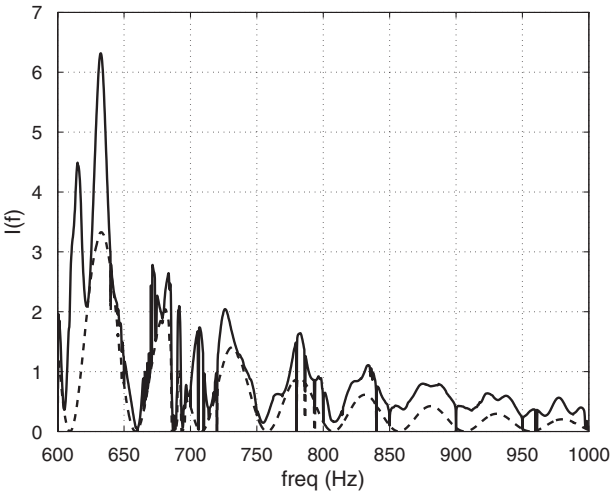

FIG. 3. Sensitivity integrands for the LIGO-only result (dashed) and for the full LIGO-Virgo result (solid). We can see that the sensitivity is increased across the band by the addition of the Virgo interferometer to the search. The vertical lines correspond to frequency bins removed from the search.

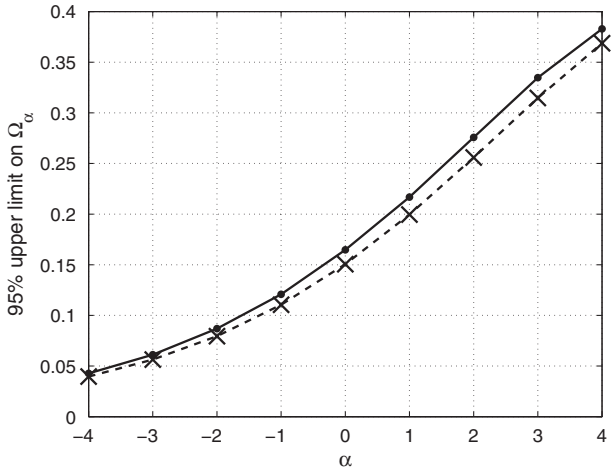

FIG. 4. 95% probability intervals on Ω_α, calculated using different values of α. These upper limits were all calculated using the same data, with a band width of 600–1000 Hz and a reference frequency of 900 Hz. The dashed line shows the upper limit calculated using the LIGO interferometers only, while the solid line shows the upper limits calculated using all of the available data. The lower limits were all zero.

limit using the whole data set, even though the sensitivity of the combined LIGO-Virgo analysis is better. This is not surprising because the addition of Virgo also increases the value of the estimator. The estimator will usually lie somewhere between 0 and 2σ-in this case, the LIGO-only estimator was in the lower part of that range while the LIGO-Virgo estimator was not, but the two results are entirely consistent with each other. When we add Virgo, the likelihood excludes more of the parameter space below $\Omega_3 = 0$, but this is a region we already exclude by setting the priors. Monte Carlo simulations show that, in the absence of a signal, the probability of the combined LIGO-Virgo upper limit being at least this much larger than the LIGO-only upper limit is 4.3%. This probability is not so small as to indicate a non-null result and we therefore conclude that the LIGO-Virgo upper limit is larger due to statistical fluctuations.

We also used the same data to calculate the 95% probability intervals for gravitational-wave spectra with spectral indices ranging over $-4 \leq \alpha \leq 4$, which correspond with different models of possible backgrounds in our frequency band. For example, a background of magnetar signals would be expected to have a spectral index of $\alpha = 4$ [3]. Figure 4 shows the values of these upper limits. Note that they were all calculated using a reference frequency of 900 Hz, and Hubble parameter $h_{100} = 0.71$.

IV. VALIDATION OF RESULTS

In order to test our analysis pipeline, we created simulated signals and used software to add them to the data that had been taken during the first week of Virgo's first science run (this week was then excluded from the full analysis). We generated frame files containing a simulated isotropic stochastic background, with $\Omega_{\mathrm{GW}}(f) \propto f^3$. We were then able to scale this signal to several values of Ω_3 and add it to the data taken from the instruments. We did not include H2 in this analysis, but used only H1, L1, and V1. Table IV shows the injected values of Ω_3 and the recovered values and associated standard deviations, along with the SNR of the signal in the H1V1 pair. The recovered 95% probability intervals of the injections can be seen in Fig. 5. The intervals all contain the injected value of Ω_3.

It should be noted that, in order to have detectable signals in this short amount of data, the larger injections are no longer in the small-signal limit. We usually make two assumptions based on this limit. The first is the approximation in Eq. (8), which only holds if the signal is much smaller than the noise, as we are ignoring terms that are first and second order in $\Omega_{\mathrm{GW}}(f)$ [13]. The second

TABLE IV. Table of values of Ω_3 for software injections, along with the recovered values, the 95% probability interval and the expected SNR of each injection in the H1V1 pair. Note that the standard deviations presented in this table are underestimated, as the injections are not in the small-signal limit, however we still recover the signals within the 95% probability intervals.

Injected Ω_3	Estimator $\hat{Y}$	95% probability interval	SNR in H1V1
2.0	1.8 ± 1.3	(0.0, 4.1)	1.3
9.7	9.1 ± 1.5	(5.7, 12.8)	6.3
20.2	19.3 ± 1.8	(14.2, 24.8)	13.3
95.1	91.1 ± 3.7	(72.3, 110.6)	62.3
203.1	194.1 ± 6.2	(154.9, 234.3)	133.1

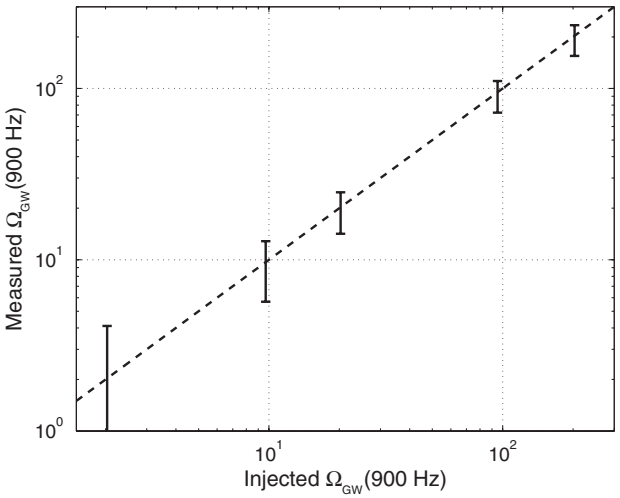

FIG. 5. Plot of the recovered values of Ω_3 for five software injections. The error bars show the 95% probability intervals. The quietest injection had a lower limit equal to zero. Note that all analyses excluded H2. Each injection used the same data, with the simulated signal scaled to different amplitudes.

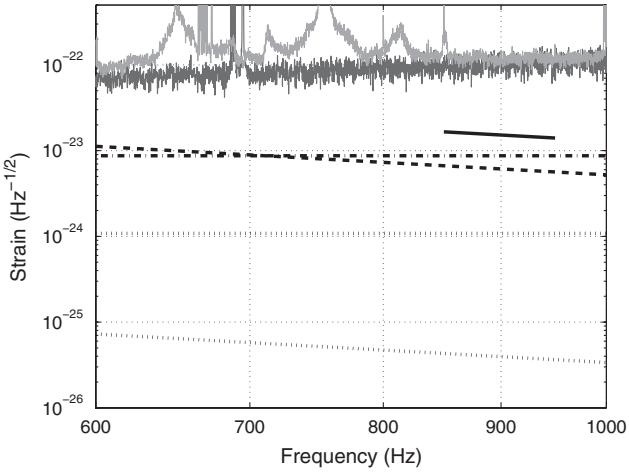

FIG. 6. Comparison of the strain sensitivity of two searches for an isotropic stochastic background of gravitational waves. The two solid grey lines show strain sensitivity of the Hanford 4 km interferometer (dark grey) and the Virgo interferometer (light grey), these spectra were obtained by averaging over the data analyzed in this paper. The dot-dashed line shows the main result of this paper, the search for a SGWB with $\Omega_{\rm GW}(f) \propto f^3$, which is white in strain amplitude, and corresponds to an upper limit of $\Omega_3 < 0.32$. The dashed line shows the result of the same search, but for constant $\Omega_{\rm GW}(f)$, and corresponds to an upper limit of $\Omega_0 < 0.16$. The solid black line shows the strain sensitivity of the LIGO-ALLEGRO search, which corresponds to an upper limit of $\Omega_0 < 1.02$ and was calculated over a frequency range of 850 Hz $\leq f \leq$ 950 Hz [18]. The two dotted lines show the extrapolation of the spectra obtained by the analysis of LIGO data in the frequency band 40 Hz $\leq f \leq$ 500 Hz. The lower dotted line corresponds to a 95% upper limit of $\Omega_0 < 6.9 \times 10^{-6}$, while the upper dotted line corresponds to an upper limit of $\Omega_3 < 0.0052$ at a reference frequency of 900 Hz.

assumption enters into the calculation of the noise PSDs, $P_i(f)$. We calculate these directly from the data, as in the small-signal limit we can assume that $\langle|\tilde{s}_i(f)|^2\rangle \approx \langle|\tilde{n}_i(f)|^2\rangle$. The first assumption causes an over-estimation of the standard deviation, while the second causes our ''optimal'' filter to no longer be quite optimal. If we ignore these assumptions, we will underestimate the theoretical error bar, σ_Y, and the width of the posterior PDFs. However, we still find 95% probability intervals that are consistent with the injected signals.

V. COMPARISON WITH OTHER RESULTS

The previous most sensitive direct upper limit in this frequency band was $\Omega_{\rm GW}(f) < 1.02$, obtained by the joint analysis of data from the LIGO-Livingston interferometer and the ALLEGRO bar detector over a frequency band of 850 Hz $\leq f \leq$ 950 Hz [18]. This result was obtained using a constant $\Omega_{\rm GW}(f) = \Omega_0$, so should be compared with our upper limit for $\alpha = 0$. As can be seen in Fig. 4, our 95% upper limit for $\alpha = 0$ is $\Omega_0 < 0.16$ using all the available data, or $\Omega_0 < 0.15$ using just the LIGO interferometers, therefore our result has improved on the sensitivity of the LIGO-ALLEGRO result by a factor of ≈ 7. The comparative strain sensitivity of the upper limits of the current search and the LIGO-ALLEGRO search can be seen in Fig. 6.

The previous most sensitive direct limit at any frequency was the analysis of data from the three LIGO detectors in the fifth science run [17]. The analysis was carried out using the same data as the analysis presented in this paper, but was restricted to the frequency band 40 Hz $\leq f \leq$ 500 Hz. This included the most sensitive frequency band of the three detectors. The 95% upper limit on Ω_0 in this band was given as 6.9×10^{-6}, which is a factor of 2×10^4 times smaller than our upper limit. They also found an upper limit on Ω_3 of 7.1×10^{-6}. In order to compare that to our upper limit on Ω_3, we must extend the spectrum to the frequency band analyzed in this paper. The 40 Hz $\leq f \leq$ 500 Hz upper limit would correspond to an upper limit at 900 Hz of $\Omega_3 < 0.0052$, which is a factor of ≈ 60 smaller than the upper limit presented in this paper. The search at lower frequencies is significantly more sensitive and we would expect that in the advanced detector era the combined analysis of LIGO and Virgo detectors at low frequencies will improve even further on the previously published upper limits.

We can also compare our results with indirect upper limits on the stochastic gravitational-wave background. In this band, the most stringent constraints come from Big Bang nucleosynthesis (BBN) and measurements of the cosmic microwave background (CMB). The BBN bound constrains the integrated energy density of gravitational waves over frequencies above 10^{-10} Hz, based on observations of different relative abundances of light nuclei today. The BBN upper limit is [6]

$$\int \Omega_{\rm GW}(f) d(\ln f) < 1.1 \times 10^{-5}(N_\nu - 3), \quad (33)$$

where N_ν is the effective number of neutrino species at the time of BBN. Recent constraints on N_ν, obtained from CMB measurements, BBN modeling, and the observed abundances of light elements suggest that $3.5 \lesssim N_\nu \lesssim 4.4$ [31–34]. The CMB limit also constrains the integrated gravitational-wave energy density, and is obtained from the observed CMB and matter power spectra, as these would be altered if there were a higher gravitational-wave energy density at the time of decoupling. The CMB upper limit [35] is

$$\int \Omega_{\rm GW}(f) d(\ln f) < 1.3 \times 10^{-5}. \quad (34)$$

Our upper limit is not sensitive enough to improve on these indirect upper limits, however, these indirect bounds only apply to a background of cosmological origin, whereas the bound presented here applies to astrophysical signals as well.

VI. CONCLUSIONS

Data acquired by the LIGO and Virgo interferometers have been analyzed to search for a stochastic background of gravitational waves. This is the first time that data from LIGO and Virgo have been used jointly for such a search, and we have demonstrated that the addition of Virgo increases the sensitivity of the search significantly, reducing the error bar by 23% even though the length of time for which Virgo was taking data was approximately one fifth of the time of the LIGO run. The upper limit obtained with the LIGO interferometers only is the most sensitive direct result in this frequency band to date, improving on the previous best limit, set with the joint analysis of ALLEGRO and LIGO data, by a factor of ≈ 7.

Adding Virgo improves the sensitivity across the frequency band, largely due to the addition of pairs which have different overlap reduction functions. This enables us to cover the frequency band more evenly, as well as effectively increasing the total observation time. We can see that the sensitivity of the search is much improved by adding Virgo by comparing the standard deviations in Table III. However, in this case, the increased sensitivity did not lead to a decreased upper limit, as the joint estimator of Ω_3 obtained by the full LIGO-Virgo search was higher than the estimator obtained by the LIGO-only analysis.

As part of this analysis, we have also developed a method of marginalizing over the error on the amplitude calibration of several interferometers. The methods used in this paper will be useful for future analyses of data from the network of interferometers, which we expect to grow, eventually including not only interferometers in North America and Europe, but also hopefully around the world.

ACKNOWLEDGMENTS

The authors gratefully acknowledge the support of the United States National Science Foundation for the construction and operation of the LIGO Laboratory, the Science and Technology Facilities Council of the United Kingdom, the Max-Planck-Society, and the State of Niedersachsen/Germany for support of the construction and operation of the GEO600 detector, and the Italian Istituto Nazionale di Fisica Nucleare and the French Centre National de la Recherche Scientifique for the construction and operation of the Virgo detector. The authors also gratefully acknowledge the support of the research by these agencies and by the Australian Research Council, the International Science Linkages program of the Commonwealth of Australia, the Council of Scientific and Industrial Research of India, the Istituto Nazionale di Fisica Nucleare of Italy, the Spanish Ministerio de Educación y Ciencia, the Conselleria d'Economia Hisenda i Innovació of the Govern de les Illes Balears, the Foundation for Fundamental Research on Matter supported by the Netherlands Organisation for Scientific Research, the Polish Ministry of Science and Higher Education, the FOCUS Programme of Foundation for Polish Science, the Royal Society, the Scottish Funding Council, the Scottish Universities Physics Alliance, The National Aeronautics and Space Administration, the Carnegie Trust, the Leverhulme Trust, the David and Lucile Packard Foundation, the Research Corporation, and the Alfred P. Sloan Foundation. This is LIGO document LIGO-P1000128.

[1] T. Regimbau and J. A. de Freitas Pacheco, Astrophys. J. **642**, 455 (2006).
[2] T. Regimbau and J. A. de Freitas Pacheco, Astron. Astrophys. **376**, 381 (2001).
[3] T. Regimbau and J. A. de Freitas Pacheco, Astron. Astrophys. **447**, 1 (2006).
[4] V. Ferrari, S. Matarrese, and R. Schneider, Mon. Not. R. Astron. Soc. **303**, 247 (1999).
[5] L. Grishchuk, JETP Lett. **23**, 293 (1976), http://www.jetpletters.ac.ru/ps/1801/article_27514.shtml.
[6] M. Maggiore, Phys. Rep. **331**, 283 (2000).
[7] X. Siemens, V. Mandic, and J. Creighton, Phys. Rev. Lett. **98**, 111101 (2007).
[8] R. Bar-Kana, Phys. Rev. D **50**, 1157 (1994).
[9] A. A. Starobinsky, JETP Lett. **30**, 682 (1979), http://www.jetpletters.ac.ru/ps/1370/article_20738.shtml.

[10] R. Brustein *et al.*, Phys. Lett. B **361**, 45 (1995).
[11] V. Mandic and A. Buonanno, Phys. Rev. D **73**, 063008 (2006).
[12] R. Apreda *et al.*, Nucl. Phys. **B631**, 342 (2002).
[13] B. Allen and J. D. Romano, Phys. Rev. D **59**, 102001 (1999).
[14] B. P. Abbott *et al.*, Rep. Prog. Phys. **72**, 076901 (2009).
[15] F. Acernese *et al.*, Classical Quantum Gravity **25**, 114045 (2008).
[16] H. Grote for the LIGO Scientific Collaboration, Classical Quantum Gravity **25**, 114043 (2008).
[17] B. P. Abbott *et al.*, Nature (London) **460**, 990 (2009).
[18] B. Abbott *et al.*, Phys. Rev. D **76**, 022001 (2007).
[19] B. Abbott *et al.*, Astrophys. J. **659**, 918 (2007).
[20] E. E. Flanagan, Phys. Rev. D **48**, 2389 (1993).
[21] N. Christensen, Phys. Rev. D **46**, 5250 (1992).
[22] G. Cella *et al.*, Classical Quantum Gravity **24**, S639 (2007).
[23] A. Lazzarini and J. R. Romano, LIGO Technical Document Report No. T040089-00, 2004, https://dcc.ligo.org/cgi-bin/DocDB/ShowDocument?docid=t040089.
[24] W. Anderson *et al.*, Tech. Report No. VIR-0416A-10, 2010, https://tds.ego-gw.it/ql/?c=7701.
[25] M. Rakhmanov, J. D. Romano, and J. T. Whelan, Classical Quantum Gravity **25**, 184017 (2008).
[26] J. Abadie *et al.*, Nucl. Instrum. Methods Phys. Res., Sect. A **624**, 223 (2010).
[27] T. Accadia *et al.*, J. Phys. Conf. Ser. **228**, 012015 (2010).
[28] N. V. Fotopoulos (for the LIGO Scientific Collaboration), J. Phys. Conf. Ser. **122**, 012032 (2008).
[29] WMAP, Wmap-recommended parameters constraints (2012), http://lambda.gsfc.nasa.gov/product/map/current/best_params.cfm.
[30] A. G. Riess *et al.*, Astrophys. J. **730**, 119 (2011).
[31] G. Manganao and P. D. Sperico, Phys. Lett. B **701**, 296 (2011).
[32] J. Hamann, S. Hannestad, G. G. Raffelt, and Y. Y. Y. Wong, J. Cosmol. Astropart. Phys. 09 (2011) 034.
[33] K. M. Nollett and G. P. Holder, arXiv:1112.2683.
[34] R. H. Cyburt *et al.*, Astropart. Phys. **23**, 313 (2005).
[35] T. L. Smith, E. Pierpaoli, and M. Kamionkowski, Phys. Rev. Lett. **97**, 021301 (2006).
[36] J. T. Whelan, E. L. Robinson, J. D. Romano, and E. H. Thrane, arXiv:1205.3112.